Theoretical realization of fully spin-polarized nodal box with traversing Brillouin zone surface state

Tingli He,[1,2] Xiaoming Zhang,[1,2,*] Lirong Wang,[1,2] Ying Liu,[1,2] Xuefang Dai,[1,2] Liying Wang,[3] and Guodong Liu[1,2,†]

[1]*State Key Laboratory of Reliability and Intelligence of Electrical Equipment, Hebei University of Technology, Tianjin 300130, China*

[2]*School of Materials Science and Engineering, Hebei University of Technology, Tianjin 300130, China*

[3]*Tianjin Key Laboratory of Low Dimensional Materials Physics and Preparation Technology, School of science, Tianjin University, Tianjin 300354, People's Republic of China*

(Received 30 August 2021; revised 26 July 2022; accepted 22 August 2022; published 30 August 2022)

Magnetic topological materials have attracted much attention because of their exotic topological quantum physics arising from the interplay between spintronics, crystallography, magnetism, and topology. Based on first-principles calculations and crystal symmetry analysis, we present a lot of materials with fully spin-polarized nodal boxes in a ferromagnetic cubic structure. This nodal box is formed by six butterflylike nodal lines in the Brillouin zone when neglecting the weak spin-orbit coupling (SOC) mainly from F atoms. Such a fully spin-polarized nodal box is reported here. The M_{110} mirror symmetry is not broken in [110] magnetization direction, thus leaving a symmetrically protected butterflylike nodal line on the (110) surface when the SOC is present. The band gaps of the nodal box induced by SOC are less than 1 meV due to the weak SOC effect. Our discovery fills the gap in the study of a fully spin-polarized nodal box in the magnetic system and provides a good research platform for studying the combination of new topological states and spintronics. Such a fully spin-polarized nodal box with unique Fermi surfaces and surface states traversing the Brillouin zone holds great promise for applications in catalysis and spin transport.

DOI: 10.1103/PhysRevB.106.075155

I. INTRODUCTION

Topological semimetals/metals (TSMs) hosting a finite number or continuous nodal line of band crossings near the Fermi level in momentum space have attracted widespread attention [1–8]. In physics, the study of TSMs indicates that Fermi surfaces crossed by conduction and valence bands in momentum space can exhibit different patterns, such as points [9–13], lines [14–24], and surfaces [25–29]. Compared to nodal points, nodal lines are more flexible to form various topological states. Many interesting physical properties have been proposed in these interesting nodal line materials, such as drumhead states [30], Friedel oscillation [31], nondispersive Landau energy levels [32], specific long-range Coulomb interactions [33], and so on. In particular, the nodal lines in magnetic materials represent a different type. It will be most interesting when the material is half metallic. Half metals exhibit one spin channel possessing a metallic state while the other remains in an insulating or semiconducting state. Different from conventional ferromagnetic (FM) compounds with a low degree of spin polarization, half metals with 100% spin polarization are considered to be excellent candidates for spintronics. Thus all the interesting physical properties related to the nodal lines occur in only one single spin and the spin polarization can be switched by controlling the magnetization direction [34–36]. Therefore, researchers strive to find new topological phases in magnetic systems and try to reveal new topological properties and application prospects in magnetic systems.

Nodal lines can be formed in various forms flexibly, such as nodal rings [8,19,37–40], nodal chains [19,26,41–44], nodal knots [45–47], nodal nets [48,49], nodal link [50], nodal box [51], and Hopf chains [50,52–54] based on the shape of the nodal lines. So far, different types of nodal lines in the model or nonmagnetic system have been proposed. So far, many types of nodal line TSMs have been predicted. But the reported nodal lines in the magnetic system are very limited. Moreover, the types of nodal line reported in the magnetic system are mainly simple nodal line or nodal ring [34,55,56]. Recently, nodal chain has been proposed in the magnetic materials Co_2MnGa [57], $XTiMn(PO_4)_3$ (X = Ca, Mg, Zn) [58], and LiV_2O_4 [59]. A topological phase namely nodal box, where the crossing among nodal lines shows the boxlike configuration protected by C_3 symmetry, has been recently proposed in nonmagnetic material CuAgSe [51]. It shows unique topological characteristics and transport properties different from isolated and intersecting rings. However, the nodal box was reported in the nonmagnetic system [51]. The system with magnetic properties will have great prospects for applications in spintronics, which can carry information not only by charge, but also one by spin. Half metals with 100% spin polarization are considered to be excellent spintronics candidates for spin generation, injection, and transport. Therefore, exploring a new family of nodal box in ferromagnetic half metals is crucial in boosting the development of spintronic devices. We look for nodal boxes very close to the Fermi energy level in ferromagnetic half metals, which gives the system a large electron mobility and a highly tunable ability

*zhangxiaoming87@hebut.edu.cn
†gdliu1978@126.com

to use external fields such as pressure, electric field, magnetic field, electromagnetic radiation, etc.

In this work, we found a symmetry-enforced butterfly nodal line in ferromagnetic Cs_2AF_6 (A = Ag, Cu) compounds. Specific butterfly nodal line features are protected by M_{110} mirror symmetry on the (110) surface. Considering the six mirror symmetries in the O_h point group, the butterflylike nodal lines form a nodal box in the Brillouin zone (BZ). In these half-metallic ferromagnets, the nodal boxes are fully spin polarized, which is very different from the previously reported nodal box in a nonmagnetic system. Moreover, the surface states of the nodal box traverse the entire BZ, which will be very beneficial for the experimental observation. When the SOC is present, the M_{110} mirror symmetry is present when the magnetization is along the [110] direction, thus leaving a symmetrically protected butterflylike nodal line on the (110) surface. The band gaps of a nodal box induced by SOC are less than 1 meV due to the weak SOC effect. Using high-throughput calculations, we also predict that a class of materials X_2YZF_6 (X = Rb, K, Cs, Na; Y= Na, Li; Z = Ni, Pd) possess the same nodal box topology features. Through our analysis, we propose that a cubic structure with $Fm\bar{3}m$ space group can host an ideal nodal-box structure when the weak SOC effect is neglected. Our work presents a large number of half-metallic ferromagnets with nodal-box properties, providing a good platform for research in spintronics and topological physics.

II. COMPUTATIONAL DETAILS

The first-principles calculations were performed by using the Vienna *ab initio* Simulation Package [60,61]. The correlation potential is chosen as the generalized gradient approximation (GGA) with Perdew Burke, and Ernzerhof (PBE) [62]. The plane-wave basis set with an energy cutoff of 500 eV was used. The Brillouin zone was sampled by a Monkhorst-Pack [63] k mesh with a size of $15 \times 15 \times 15$. Energy and force convergence criteria were set as 10^{-7} eV and 0.001 eV/Å, respectively. To account for the correlation effects for transition-metal elements of the Ag atom, we applied the GGA+U method [64]. The effective U value for Ag was chosen as 3 eV. Note that shifting the U values will not change the conclusion of our work. The graph of electronic band structure and projected density of states is plotted by the PYMATGEN package [65]. The surface states are calculated by using the WANNIERTOOLS package [66]. The irreducible representations of the electronic states are obtained by using the IRVSP code [67].

III. RESULTS AND DISCUSSIONS

A. Crystal structure and magnetic properties in Cs_2AF_6 (A = Ag, Cu) compounds

The lattice structure for the Cs_2AF_6 (A = Ag, Cu) compounds is shown in Fig. 1(a). They crystallize in the cubic K_2PtCl_6-type structure with space group $Fm\bar{3}m$ (No. 225). The Cs atoms are located at 8c (0.25, 0.24, 0.25), A at 4a (0, 0, 0), and F at 24e (x, 0, 0) Wyckoff sites. This structure is characterized by two structural parameters that are not fixed by symmetry: the lattice parameter a and the position of the F atom (x, 0, 0), which can be determined by relaxing the lattice. Figure 1 shows the conventional lattice of Cs_2AF_6 (A = Ag, Cu). These compounds can be seen as AF_6 octahedra well separated by the presumed inert Cs ions, which serve to fill the space and give charge to the AF_6 unit. We used Cs_2AgF_6 as a representative of the Cs_2AF_6 (A = Ag, Cu) series studied. The equilibrium lattice parameter of the Cs_2AgF_6 compound is $a = b = c = 9.25$ Å, which is consistent with the experimental lattice parameter $a = b = c = 9.010 \pm 0.005$ Å [68]. Since the cubic symmetry in Cs_2AgF_6 is crucial for the discussions in the following, we here further verify the stability of cubic Cs_2AgF_6 from the phonon calculation. As shown in Fig. 1(c), the phonon spectrum exhibit no imaginary frequency mode throughout the Brillouin zone, indicating cubic Cs_2AgF_6 is indeed dynamically stable.

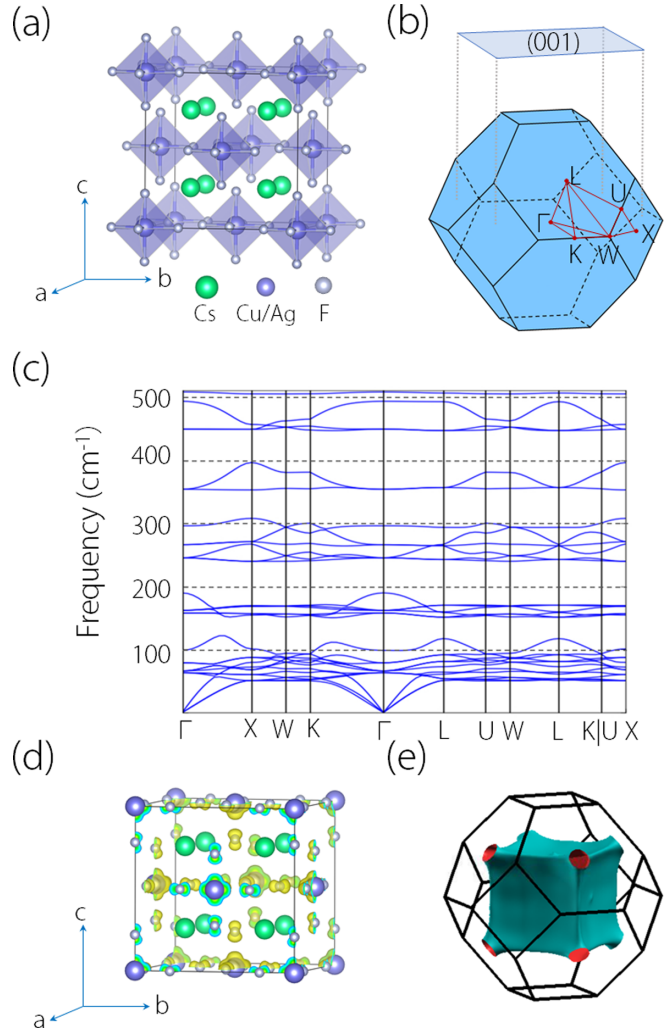

FIG. 1. (a) Conventional cell of Cs_2AF_6 (A = Ag, Cu) compounds. (b) The bulk Brillouin zone (BZ) with the high symmetry points labeled and (001) plane surface BZ. (c) Calculated phonon spectrum of cubic Cs_2AgF_6 along high symmetry k path in the bulk BZ. (d) Three-dimensional magnetic charge density (yellow) of Cs_2AgF_6. (e) The Fermi surface with electron (red) and hole (blue) pockets.

Figure 1(d) depicts the three-dimensional (3D) spin-difference density of Cs_2AgF_6. It is clearly observed that the

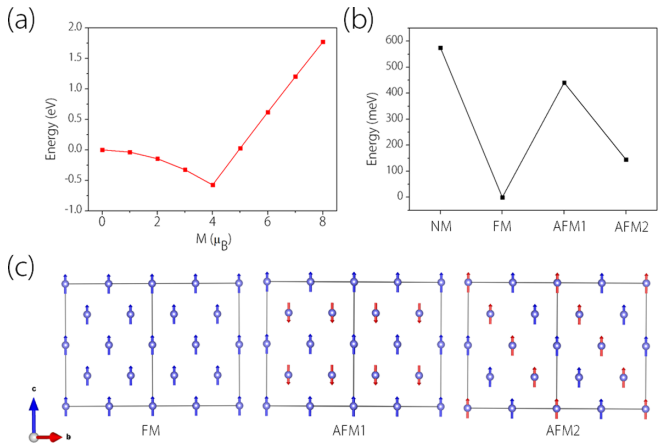

FIG. 2. (a) Total energy of fixed spin moment changes in the Cs_2AgF_6 unit cell. (b) Comparison of the energy among the different magnetic states; the FM state was set as the reference energy. (c) FM and AFM states in a $2 \times 2 \times 2$ supercell of Cs_2AgF_6. Only Ag atoms are shown here.

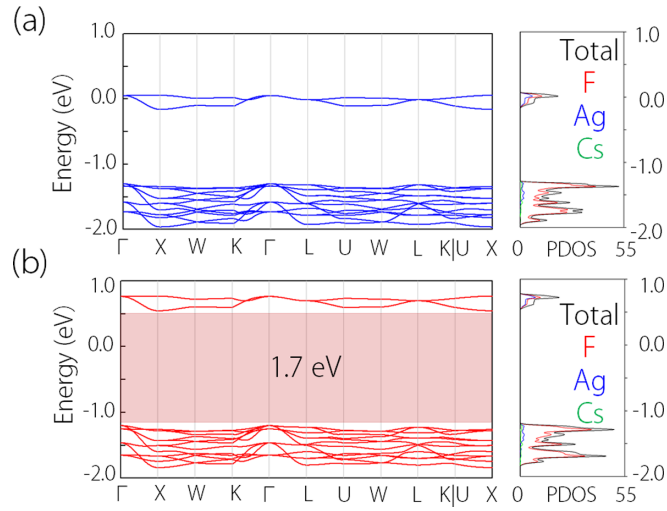

FIG. 3. Electronic band structure and the projected density of states of Cs_2AgF_6 in (a) spin-up channel and (b) spin-down channel. Black represents the total density of states, red is the density of states of F atoms, blue is the density of states of Ag atoms, and green is the density of states of Cs atoms in the right side of the figure.

magnetic moments are mainly distributed around Ag and the magnetic moment of per unit cell is $4\mu_B$. In other words, the magnetic moment of the Cs_2AgF_6 compound is $1\mu_B$ per primitive cell. Experimentally, we found that Cs_2AgF_6 was shown to be weakly magnetic [68], indicating that it may be the ferromagnetic behavior at low temperature. To understand its magnetic properties, we fixed the magnetic moment to compare the energies. As can be seen in Fig. 2(a), there is a considerable nonmagnetic instability. The magnetic ground state of Cs_2AgF_6 was evaluated by constructing nonmagnetic (NM), ferromagnetic (FM), and antiferromagnetic (AFM) configurations. Two different types of antiferromagnetic structures (AFM1 and AFM2) are considered, as shown Fig. 2(c). By comparing the energy of nonmagnetic, ferromagnetic, and two antiferromagnetic structures (AFM1 and AFM2), we found that FM has the lowest energy from Fig. 2(b). Therefore, the FM state is most energetically stable in all magnetic configurations.

B. Nodal box in Cs_2AF_6 (A = Ag, Cu) compounds

We show the band structure of Cs_2AgF_6 based on the ferromagnetic ground state in the absence of SOC. As shown in Fig. 3, Cs_2AgF_6 exhibits a half-metallic feature with a metal in the spin-up channel and a semiconductor with a gap of 1.7 eV in the spin-down channel. The total and projected density of states (TDOSs and PDOSs) on the right side of Fig. 3 shows that the electron states near the Fermi level are dominated by F atoms. Several band crossings are observed close to the Fermi energy level in the spin-up channel and are very clean from the interference of other trivial bands. Importantly, these band crossings are fully spin polarized, which greatly increases carrier mobility.

The detailed analysis of the electronic band structure in the absence of SOC is shown in Fig. 4. In Fig. 4(a), we can observe the linear band crossing in the Γ-K path and the doubly degenerate nodal line in the Γ-L path. The nodal line along the Γ-L path is protected by point group C_{3v}. The Weyl point in the Γ-K path is protected by the point group of C_{2v} with different irreducible representation Γ_1 and Γ_4. A careful scan of the band structure around the Γ points shows that these band crossings are not isolated. Interestingly, these nodal lines and nodal points formed a butterflylike nodal line on the (110) surface protected by the M_{110} mirror symmetry [see Fig. 4(b)]. The symmetry group contains six mirror planes, collectively referred to as M_{110}. All the butterflylike nodal lines on the (110) surface combine to form a nodal box in the Brillouin

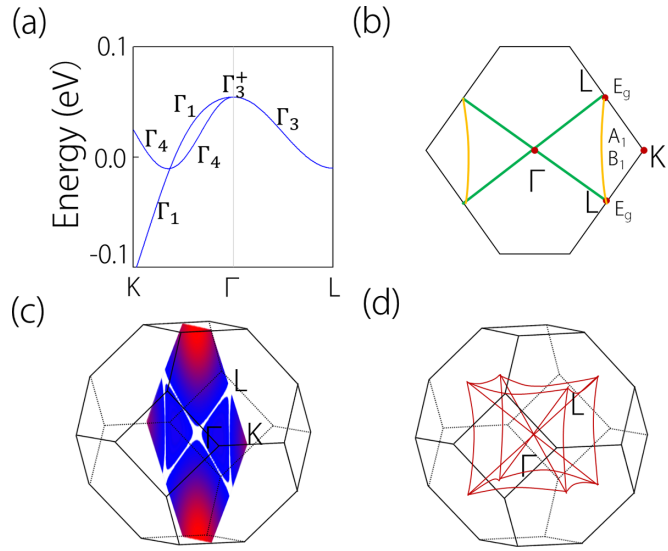

FIG. 4. (a) Enlarged band structure along the K-Γ-L. (b) Schematic diagram of four lines, with irreducible marked on the line. (c) The shape of the butterfly-shaped nodal line on one (110) plane in bulk Brillouin zone (BZ) obtained by DFT calculation. The bright white line represents the contour line where the energy difference between the two bands is zero. (d) Main view of a nodal box formed by combining all the butterfly-shaped nodal lines on the six (110) plane.

zone as shown in Figs. 4(c) and 4(d). By plotting the Fermi surface in Fig. 1(e), we find an electron pocket (red) on the corners of the nodal box and a hole pocket (blue) on the face of the nodal box. To the best of our knowledge, the nodal box structure proposed in this paper is different from the known nodal line, nodal chain, and nodal network systems. We hope that this unique nodal box structure will yield new properties in future transmission experiments.

Now we understand the nodal box from the symmetry point of view. In the Cs_2AgF_6 compound, there are only two bands near the Fermi level. It is worth noting that these two bands have two-dimensional (2D) irreducible representation Γ_3 on the Γ-L path. Therefore, a nodal line is formed on the Γ-L path. Along the Γ-K path, the two bands separate to form a crossing point. Based on the irreducible representation, we derive the effective model up to the first order of k for the crossing point along Γ-K, which is given by

$$H_{(\Gamma-K)} = [M + B_1(k_x + k_y)]\sigma_0 + [\Delta_0 - B_2(k_x + k_y)]\sigma_z + A(k_x - k_y)\sigma_x. \quad (1)$$

According to the presence of M_{110}, one could discover that this crossing point is not isolated, but rather a generic point on a nodal line on $k_x = k_y$ plane. To be specific, we consider that, up to the second order of k, the effective model for the nodal lines is given by

$$H_{NL}(k_x, k_y, k_z) = H_{(\Gamma-K)} + D_0\left(k_x^2 - k_y^2\right)\sigma_x + \left[C_0 k_z^2 - A_1\left(k_x^2 + k_y^2\right) + A_2 k_x k_y\right]\sigma_z. \quad (2)$$

Such an effective model gives rise to a crossing point in 1D on the $k_x = k_y$ plane. On this plane, one has

$$H_{NL}(k, k, k_z) = \left[\Delta_0 - 2B_2 k + C_0 k_z^2 - (2A_1 - A_2)k^2\right]\sigma_z. \quad (3)$$

If the two bands are degenerate, one has

$$\Delta_0 - 2B_2 k + C_0 k_z^2 - (2A_1 - A_2)k^2 = 0, \quad (4)$$

which leads to the solutions

$$k_z = \pm\sqrt{C_0^{-1}[k(2B_2 + 2A_1 k - 2A_2 k) - \Delta_0]}. \quad (5)$$

Hence one could derive two nodal lines on this plane, as shown by the yellow line in Fig. 4(b). The two bands near the Fermi level are 1D irreducible (A_1, B_1), and become 2D irreducible (E_g) only at the L point. Therefore, the green line and the yellow line must cross at point L. The boundary of the two nodal lines will share one L point and finally form a butterfly shaped nodal line on the (110) plane. Due to the cubic structure with O_h symmetry of the system, there are six mirror planes M_{110}. All the butterflylike nodal lines on the (110) plane combine to form a nodal box in the Brillouin zone. Similar connections of nodal lines have also been discussed in several intersecting-nodal-ring examples [19]. In addition to the advantages of standard half metals, the spin-polarized nodal box has large electron mobility and highly adjustable ability through external fields (such as pressure, electric field, magnetic field, electromagnetic radiation, etc.). The unique topological phase of spin polarization provides another platform and opportunity for spintronics, electronics, and optics.

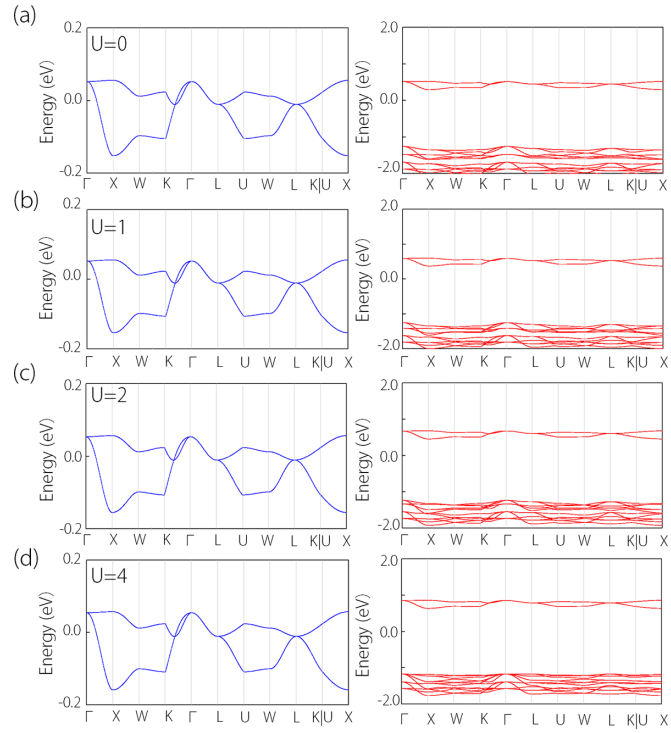

FIG. 5. (a)–(d) Band structures of Cs_2AgF_6 in the spin-up (the left panel) and spin-down (the right panel) channels with varying U (0, 1, 2, 4) values.

In particular, the spin-polarized topological phase has a nodal box with a single spin channel and no other entangled trivial bands, which combines spintronics and topological physics.

The electronic band structure of Cs_2CuF_6 is similar to that of Cs_2AgF_6. Specifically, Cs_2CuF_6 has the same band crossings as Cs_2AgF_6 in spin up channel and has a gap of 1.35 eV in spin down channel. Thus a completely polarized nodal box is also found in the Cs_2CuF_6 compound. In particular, the nodal box was previously mentioned only in the nonmagnetic system [51]. In this work, the fully polarized nodal box is proposed in a ferromagnetic system, which nicely combines spintronics and topological physics. We also show the effect of the U value on the electronic band structure and the results are shown in Figs. 5(a)–5(d), indicating that the U value does not have much effect on the electronic band structure. The band crossings in the spin-up channel still exist and do not change much in energy and momentum space.

One of the hallmarks of nontrivial topological materials is the existence of a topologically protected surface state. As mentioned above, the fully spin-polarized nodal box exists in the Cs_2AF_6 (A = Ag, Cu) compound. We can expect drumhead surface states of the fully spin-polarized nodal box. To address the issue, we have identified the surface spectrum of the (001) surface of Cs_2AgF_6. In Fig. 6(a), we depict the surface states along the high symmetry path, observing the drumhead surface states of the nodal box clearly. We observe that the drumhead surface states connected through and traverse the entire Brillouin zone. As shown in the Figs. 6(b) and 6(c), we further show the evolution of the drumheadlike surface states from the momentum space and energy space, respectively. In Fig. 6(b), the butterflylike nodal line evolves

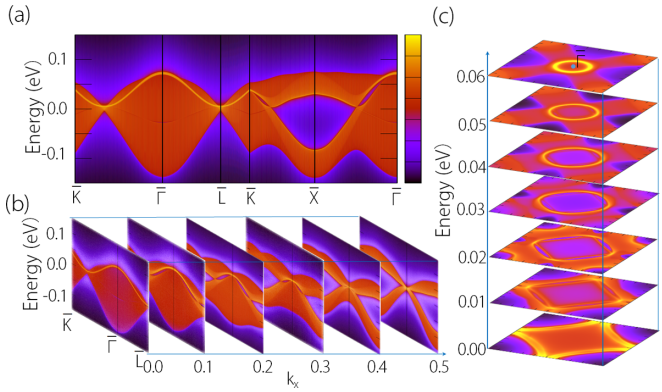

FIG. 6. (a) Surface spectrum on the (001) surface along the high symmetry line. (b) Evolution of the surface state as the value of k_x increases. (c) The energy-dependent evolution of the (001) surface state.

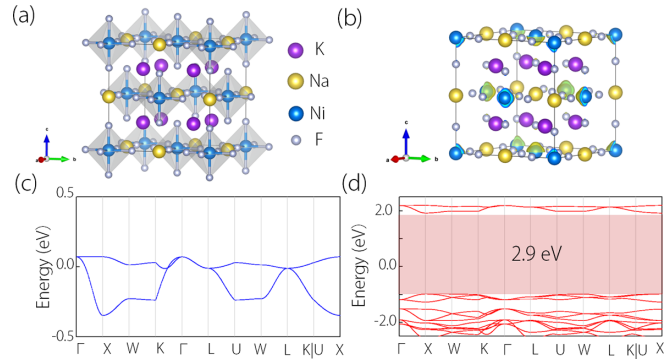

FIG. 8. (a) Conventional cell of K_2NaNiF_6 compound. (b) Three-dimensional magnetic charge density (yellow) of K_2NaNiF_6. Electronic band structure and the projected density of states of K_2NaNiF_6 in (c) spin-up channel and (d) spin-down channel.

in momentum space as k_x increases ($k_x = 0.0$–0.5). From Fig. 6(c), we can observe the evolution of the surface states on the (001) surface spectrum at different energies. When the energy range is 0.0 to 0.06, the surface state of the drum near the Γ point is clearly observed. The drumheadlike surface state with unusually high electron density near the Fermi level facilitates hydrogen precipitation from water [69–71]. The surface states traversing the Brillouin zone with high electron density are not only very favorable for experimental observations, but may also have good catalytic properties.

As can be seen from Fig. 7(a), the electronic band structure near the Fermi level is mainly contributed by F atoms. The SOC effect is not significant in its impact on electronic structure. The direction of spontaneous magnetization is determined by studying the total energy along different magnetization directions including [001], [110], and [111] axes. The results show that the [110] direction has the lowest energy, which is 0.1 meV lower than [001] and [111] axes. The electronic band structure with SOC in different magnetization directions has no change compared with those without considering SOC. The electronic band structure near the Fermi energy level is mainly contributed by F atom. Due to the weak spin-orbit coupling effect of this system, the electronic structure does not change in different magnetization directions when considering SOC. Therefore, the nodal box will not be easily damaged. Based on the symmetry analysis, the M_{110} symmetry is not broken, protecting the butterflylike nodal lines on the (110) plane [see Figs. 7(b) and 7(c)] when the magnetization direction is along [110]. Interestingly, the SOC effect is very small and only opens up the gap to less than 1 meV. Therefore, the characteristic of the nodal box is hardly affected when the SOC is considered. When the magnetization direction is along the [100] direction, the M_{110} symmetry is destroyed and the nodal line opens up the gap. However, the gap of the nodal line is less than 1 meV. Therefore, due to the weak SOC of the system, the nodal box will not be easily destroyed. Here, we would like to emphasize that the nodal box not only possesses a traversing Brillouin zone surface state, but also is fully spin polarized. The topological nodal box induced drumhead surface states and provides sufficient active planes that will favor catalysis [69–72]. Unlike conventional ferromagnetic (FM) materials with low spin polarization, fully spin-polarized nodal boxes with 100% spin polarization are considered as excellent spintronics candidates for spin generation, injection, and transport. The effective combination of nodal boxes and fully spin-polarized properties provides potential design ideas for high-performance spintronic devices. The realization of fully spin-polarized nodal-box materials has greatly expanded the topological magnetic topological family and has great application prospects in topological catalysis and spintronics [21,73–76].

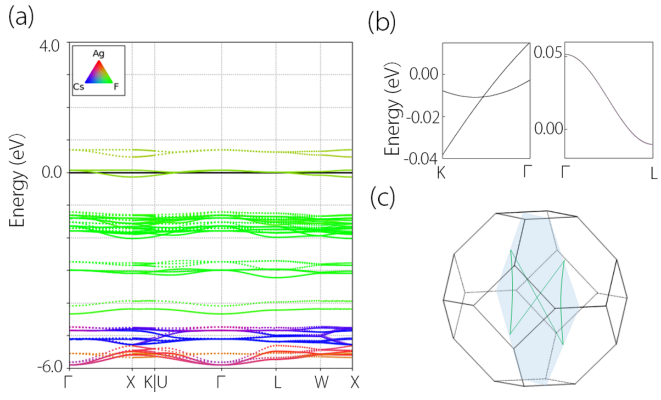

FIG. 7. (a) Electronic band structure of atomic projection. (b) Enlarged view of energy bands along K-Γ and Γ-L paths in the presence of SOC. (c) When the magnetization is along the [110] direction, the symmetrical protection of the butterflylike on the (110) plane of the nodal line in the presence of SOC.

C. Nodal box in elpasolite type compounds

As discussed above, our results indicate the existence of a fully spin-polarized nodal box in the Cs_2AF_6 (A = Ag, Cu) compounds when the weak SOC mainly from the F atoms is ignored. In addition to K_2PtCl_6-type structure, we also found that a series of compounds with elpasolite type X_2YZF_6 (X = Rb, K, Cs, Na; Y = Na, Li; Z = Ni, Pd) also have the topological properties of a nodal box through high-throughput calculation. Finally, we found 10 compounds with fully spin-polarized nodal-box properties with the $Fm\bar{3}m$

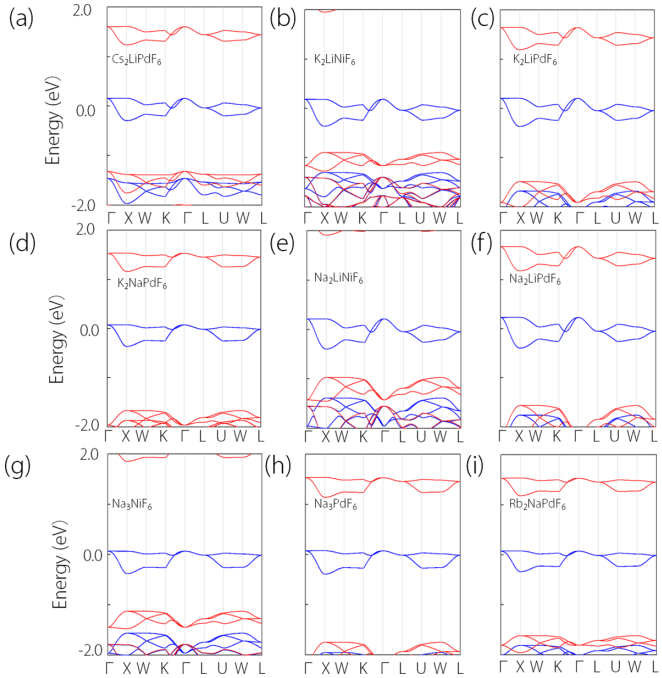

FIG. 9. (a)–(i) Electronic band structure of X_2YZF_6 (X = Rb, K, Cs, Na; Y= Na, Li; Z = Ni, Pd) (blue and red lines correspond to spin-up and spin-down channels, respectively).

space group. Their structural information comes from the Materials Project [77].

We used K_2NaNiF_6 as a representative of the X_2YZF_6 (X = Rb, K, Cs, Na; Y = Na, Li; Z = Ni, Pd) compounds studied. K_2NaNiF_6 crystallizes in the $Fm\bar{3}m$ with O_h symmetry and the Ni atom occupies perfect octahedral sites surrounded by six Cl atoms [see Fig. 8(a)]. Figure 8(b) depicts the three-dimensional (3D) magnetic charge density of K_2NaNiF_6. It is clearly observed that the magnetic moments are distributed around the Ni atoms and the calculated values of magnetic moments are $4\mu_B$ per unit cell. We clearly find the electronic band structures of the half-metallic nature and the band crossings on one spin from Figs. 8(c) and 8(d). Importantly, the band crossings along the K-Γ and Γ-L paths form butterfly-like nodal lines. Considering the six M_{110} mirrors under O_h symmetry, the butterflylike nodal line forms a nodal box in the Brillouin zone. The results of the electronic band structure for the other nine (X_2YZF_6) (X = Rb, K, Cs, Na; Y= Na, Li; Z = Ni, Pd) compounds are shown in Figs. 9(a)–9(i). We clearly find that these compounds maintain the half-metallic nature and also have the topological properties of the nodal box mentioned above.

IV. SUMMARY

In conclusion, we predict a series of materials with fully spin-polarized nodal boxes in the $Fm\bar{3}m$ structure when neglecting the weak spin-orbit coupling (SOC) mainly from F atoms by first-principles calculations and symmetry analysis. The butterfly-shaped nodal lines on the (110) face are symmetrically protected by the mirror M_{110}. The nodal-box structure consists of six butterfly-shaped nodal lines, which protect by M_{110} symmetry and cannot be removed without breaking the symmetry. In the absence of SOC, the band crossings occur in a single spin and therefore have a fully spin-polarized nodal box. When the SOC is present, the M_{110} mirror symmetry is not broken in the [110] magnetization direction, thus leaving a symmetrically protected butterflylike nodal line on the (110) surface. The band gaps of the nodal box induced by SOC are less than 1 meV due to the weak SOC effect. Our work proposes a series of fully spin-polarized nodal box materials, which show great application potential in spintronics, topology, and catalysis due to their unique Fermi surface and surface states that traverse the Brillouin zone.

ACKNOWLEDGMENTS

This work is supported by the National Natural Science Foundation of China (Grant No. 11904074). The work is funded by Science and Technology Project of Hebei Education Department, the Nature Science Foundation of Hebei Province, S&T Program of Hebei (Grant No. A2021202012), the Overseas Scientists Sponsorship Program by Hebei Province (Grants No. C20200319 and No. C20210330), and the Doctoral Postgraduate Innovation Funding project of Hebei Province (Grant No. CXZZSS2022050). The work is also supported by the State Key Laboratory of Reliability and Intelligence of Electrical Equipment (Grant No. EERI_-OY2020001), Hebei University of Technology. One of the authors (X.M.Z.) acknowledges the financial support from Young Elite Scientists Sponsorship Program by Tianjin.

[1] N. P. Armitage, E. J. Mele, and A. Vishwanath, Rev. Mod. Phys. **90**, 015001 (2018).
[2] H. Weng, X. Dai, and Z. Fang, J. Phys.: Condens. Matter **28**, 303001 (2016).
[3] M. Z. Hasan, S.-Y. Xu, and B. Guang, Phys. Scr. **T164**, 014001 (2015).
[4] B. Yan and C. Felser, Annu. Rev. Condens. Matter Phys. **8**, 337 (2017).
[5] M. Hirayama, R. Okugawa, and S. Murakami, J. Phys. Soc. Jpn. **87**, 041002 (2018).
[6] A. A. Burkov, M. D. Hook, and L. Balents, Phys. Rev. B **84**, 235126 (2011).
[7] C.-K. Chiu and A. P. Schnyder, Phys. Rev. B **90**, 205136 (2014).
[8] C. Fang, Y. Chen, H.-Y. Kee, and L. Fu, Phys. Rev. B **92**, 081201 (2015).
[9] H. B. Nielsen and M. Ninomiya, Phys. Lett. B **130**, 389 (1983).
[10] L. Balents, Physics **4**, 36 (2011).
[11] X. Wan, A. M. Turner, A. Vishwanath, and S. Y. Savrasov, Phys. Rev. B **83**, 205101 (2011).
[12] G. Xu, H. Weng, Z. Wang, X. Dai, and Z. Fang, Phys. Rev. Lett. **107**, 186806 (2011).
[13] A. A. Soluyanov, D. Gresch, Z. Wang, Q. Wu, M. Troyer, X. Dai, and B. A. Bernevig, Nature (London) **527**, 495 (2015).

[14] S. Kobayashi, Y. Yamakawa, A. Yamakage, T. Inohara, Y. Okamoto, and Y. Tanaka, Phys. Rev. B **95**, 245208 (2017).

[15] S. Li, Z.-M. Yu, Y. Liu, S. Guan, S.-S. Wang, X. Zhang, Y. Yao, and S. A. Yang, Phys. Rev. B **96**, 081106(R) (2017).

[16] J. Wang, Phys. Rev. B **96**, 081107(R) (2017).

[17] R.-W. Zhang, C.-C. Liu, D.-S. Ma, M. Wang, and Y. Yao, Phys. Rev. B **98**, 035144 (2018).

[18] D.-S. Ma, J. Zhou, B. Fu, Z.-M. Yu, C.-C. Liu, and Y. Yao, Phys. Rev. B **98**, 201104(R) (2018).

[19] C. Gong, Y. Xie, Y. Chen, H.-S. Kim, and D. Vanderbilt, Phys. Rev. Lett. **120**, 106403 (2018).

[20] X. Wang, Phys. Rev. Lett. **100**, 156404 (2008).

[21] T. He, X. Zhang, L. Wang, Y. Liu, X. Dai, L. Wang, and G. Liu, Mater. Today Phys. **17**, 100360 (2021).

[22] B. Fu, X. Fan, D. Ma, C.-C. Liu, and Y. Yao, Phys. Rev. B **98**, 075146 (2018).

[23] B. Singh, B. Ghosh, C. Su, H. Lin, A. Agarwal, and A. Bansil, Phys. Rev. Lett. **121**, 226401 (2018).

[24] L. M. Schoop, M. N. Ali, C. Straer, A. Topp, A. Varykhalov, D. Marchenko, V. Duppel, S. S. P. Parkin, B. V. Lotsch, and C. R. Ast, Nat. Commun. **7**, 11696 (2016).

[25] Q.-F. Liang, J. Zhou, R. Yu, Z. Wang, and H. Weng, Phys. Rev. B **93**, 085427 (2016).

[26] T. Bzdušek and M. Sigrist, Phys. Rev. B **96**, 155105 (2017).

[27] S. A. Yang, SPIN **06**, 1640003 (2016).

[28] X. Zhang, Z.-M. Yu, Z. Zhu, W. Wu, S.-S. Wang, X.-L. Sheng, and S. A. Yang, Phys. Rev. B **97**, 235150 (2018).

[29] C. Zhong, Y. Chen, Y. Xie, S. A. Yang, M. L. Cohen, and S. B. Zhang, Nanoscale **8**, 7232 (2016).

[30] H. Weng, Y. Liang, Q. Xu, R. Yu, Z. Fang, X. Dai, and Y. Kawazoe, Phys. Rev. B **92**, 045108 (2015).

[31] R. Li, H. Ma, X. Cheng, S. Wang, D. Li, Z. Zhang, Y. Li, and X.-Q. Chen, Phys. Rev. Lett. **117**, 096401 (2016).

[32] J.-W. Rhim and Y. B. Kim, Phys. Rev. B **92**, 045126 (2015).

[33] Y. Huh, E.-G. Moon, and Y. B. Kim, Phys. Rev. B **93**, 035138 (2016).

[34] C. Chen, Z.-M. Yu, Si Li, Z. Chen, X.-L. Sheng, and S. A. Yang, Phys. Rev. B **99**, 075131 (2019).

[35] Y. Jiao, F. Ma, C. Zhang, J. Bell, S. Sanvito, and A. Du, Phys. Rev. Lett. **119**, 016403 (2017).

[36] Z. Wang, M. G. Vergniory, S. Kushwaha, M. Hirschberger, E. V. Chulkov, A. Ernst, N. P. Ong, R. J. Cava, and B. A. Bernevig, Phys. Rev. Lett. **117**, 236401 (2016).

[37] K. Mullen, B. Uchoa, and D. T. Glatzhofer, Phys. Rev. Lett. **115**, 026403 (2015).

[38] Y. Chen, Y. Xie, S. A. Yang, H. Pan, F. Zhang, M. L. Cohen, and S. Zhang, Nano Lett. **15**, 6974 (2015).

[39] Y. Gao, Y. Chen, Y. Xie, P.-Y. Chang, M. L. Cohen, and S. Zhang, Phys. Rev. B **97**, 121108(R) (2018).

[40] X. Wang, G. Ding, Z. Cheng, X. L. Wang, and G. Zhang, J. Mater. Chem. C **8**, 5461 (2020).

[41] R. Yu, Q. Wu, Z. Fang, and H. Weng, Phys. Rev. Lett. **119**, 036401 (2017).

[42] S.-S. Wang, Y. Liu, Z.-M. Yu, X.-L. Sheng, and S. A. Yang, Nat. Commun. **8**, 1844 (2017).

[43] Q. Yan, R. Liu, Z. Yan, B. Liu, H. Chen, Z. Wang, and L. Lu, Nat. Phys. **14**, 461 (2018).

[44] J. Cai, Y. Xie, P.-Y. Chang, H.-S. Kim, and Y. Chen, Phys. Chem. Chem. Phys. **20**, 21177 (2018).

[45] M. R. Dennis, R. P. King, B. Jack, K. O'Holleran, and M. J. Padgett, Nat. Phys. **6**, 118 (2010).

[46] M. Ezawa, Phys. Rev. B **96**, 041202(R) (2017).

[47] R. Bi, Z. Yan, L. Lu, and Z. Wang, Phys. Rev. B **96**, 201305(R) (2017).

[48] J.-T. Wang, S. Nie, H. Weng, Y. Kawazoe, and C. Chen, Phys. Rev. Lett. **120**, 026402 (2018).

[49] X. Feng, C. Yue, Z. Song, Q. S. Wu, and B. Wen, Phys. Rev. Materials **2**, 014202 (2018).

[50] Z. Yan, R. Bi, H. Shen, L. Lu, S. C. Zhang, and Z. Wang, Phys. Rev. B **96**, 041103(R) (2017).

[51] X. L. Sheng, Z. M. Yu, R. Yu, H. Weng, and S. A. Yang, J. Phys. Chem. Lett. **8**, 3506 (2017).

[52] Y. Xie, J. Cai, J. Kim, P.-Y. Chang, and Y. Chen, Phys. Rev. B **99**, 165147 (2019).

[53] Y. Zhou, F. Xiong, X. Wan, and J. An, Phys. Rev. B **97**, 155140 (2018).

[54] C. Zhong, Y. Chen, Z. M. Yu, Y. Xie, H. Wang, S. A. Yang, and S. Zhang, Nat. Commun. **8**, 15641 (2017).

[55] Y. J. Jin, R. Wang, Z. J. Chen, J. Z. Zhao, Y. J. Zhao, and H. Xu, Phys. Rev. B **96**, 201102(R) (2017).

[56] W. Z. Meng, X. M. Zhang, Y. Liu, X. F. Dai, and G. D. Liu, Phys. Rev. B **104**, 195145 (2021).

[57] G. Chang, S.-Y. Xu, X. Zhou, S.-M. Huang, B. Singh, B. Wang, I. Belopolski, J. Yin, S. Zhang, A. Bansil *et al.*, Phys. Rev. Lett. **119**, 156401 (2017).

[58] R.-W. Zhang, Z. Zhang, C.-C. Liu, and Y. Yao, Phys. Rev. Lett. **124**, 016402 (2020).

[59] H. Zhang, X. Zhang, Y. Liu, X. Dai, G. Chen, and G. Liu, Phys. Rev. B **102**, 195124 (2020).

[60] G. Kresse and J. Hafner, Phys. Rev. B **49**, 14251 (1994).

[61] G. Kresse and J. Furthmüller, Phys. Rev. B **54**, 11169 (1996).

[62] J. P. Perdew, K. Burke, and M. Ernzerhof, Phys. Rev. Lett. **77**, 3865 (1996).

[63] H. J. Monkhorst and J. D. Pack, Phys. Rev. B **13**, 5188 (1976).

[64] S. Grimme, J. Comput. Chem. **27**, 1787 (2006).

[65] S. P. Ong, W. D. Richards, A. Jain, G. Hautier, M. Kocher, S. Cholia, D. Gunter, V. L. Chevrier, K. A. Persson, and C. Gerbrand, Comput. Mater. Sci. **68**, 314 (2013).

[66] N. Marzari and D. Vanderbilt, Phys. Rev. B **56**, 12847 (1997).

[67] J. C. Gao, Q. S. Wu, C. Persson, and Z. J. Wang, Comput. Phys. Commun. **261**, 107760 (2021).

[68] P. Sorbe, J. Grannec, J. Portier, and P. Hagenmuller, J. Fluorine Chem. **11**, 243 (1978).

[69] J. X. Li, H. Ma, Q. Xie, S. B. Feng, S. Ullah, R. H. Li, J. H. Dong, D. Z. Li, Y. Y. Li, and X. Q. Chen, Sci. China Mater. **61**, 23 (2018).

[70] C. R. Rajamathi, U. Gupta, N. Kumar, H. Yang, Y. Sun, V. Suss, C. Shekhar, M. Schmidt, H. Blumtritt, P. Werner, B. H. Yan, S. Parkin, C. Felser, and C. N. R. Rao, Adv. Mater. **29**, 1606202 (2017).

[71] W. Liu, X. Zhang, W. Meng, Y. Liu, X. Dai, and G. Liu, iScience **25**, 103543 (2022).

[72] H. Chen, W. Zhu, D. Xiao, and Z. Zhang, Phys. Rev. Lett. **107**, 056804 (2011).

[73] T. He, X. Zhang, Y. Liu, X. Dai, G. Liu, Z.-M. Yu, and Y. Yao, Phys. Rev. B **102**, 075133 (2020).

[74] J.-Y. You, C. Chen, Z. Zhang, X.-L. Sheng, S. A. Yang, and G. Su, Phys. Rev. B **100**, 064408 (2019).

[75] Q. Wang, Y. Xu, R. Lou, Z. Liu, M. Li, Y. Huang, D. Shen, H. Wen, S. Wang, and H. Lei, Nat. Commun. **9**, 3681 (2018).

[76] R. W. Zhang, X. Zhou, Z. Zhang, D. S. Ma, Z. M. Yu, W. Feng, and Y. Yao, Nano Lett. **21**, 8749 (2021).

[77] A. Jain, S. P. Ong, G. Hautier, W. Chen, W. D. Richards, S. Dacek, S. Cholia, D. Gunter, D. Skinner, G. Ceder, and K. A. Persson, APL Mater. **1**, 011002 (2013).